

S2P-Net: A Spectral-Spatial Polar Network for Rotation-Invariant Object Recognition in Low-Data Regimes

Albert Heruth
Unaffiliated Researcher
Heide, Schleswig-Holstein, Germany
albert.heruth@gmail.com

April 2026

Abstract

We present **S2P-Net** (Spectral-Spatial Polar Network), a compact deep learning architecture that achieves mathematically guaranteed rotation invariance without data augmentation. The key insight is a well-known property of the discrete Fourier transform: rotating an image corresponds to a phase shift in its frequency representation, leaving the magnitude spectrum unchanged. S2P-Net exploits this property by (1) transforming the input image into polar coordinates via a differentiable, parameter-free mapping, (2) computing the one-dimensional Real FFT along the angular axis, and (3) extracting a compact spectral feature vector through pooling. A lightweight MLP trained on this representation contains only **6,564 trainable parameters**—a $323\times$ reduction compared to our CNN baseline with 2,121,316 parameters. We evaluate both architectures in two settings on an industrial parts dataset of 80 images across four categories. Under *full-data training with rotation augmentation*, both models reach 100% accuracy on all 12 rotation test angles. Under a challenging *low-data setting without rotation augmentation* (3 training images per class), S2P-Net achieves 71.2% mean accuracy with a standard deviation of only 1.6% across all angles, while the CNN baseline averages 60.0% with a standard deviation of 22.9% and collapses to 19.1% at 180° . These results demonstrate that mathematical inductive bias eliminates the need for rotation augmentation in low-data regimes, offering a principled path toward data-efficient industrial recognition systems.

1 Introduction

Object recognition in industrial settings—parts sorting, pick-and-place robotics, quality inspection—frequently faces two simultaneously difficult constraints. First, training data is scarce: collecting and labeling thousands of images for every new part type is expensive and time-consuming. Second, objects appear on conveyor belts or work surfaces in arbitrary orientations that cannot be controlled. Standard convolutional neural networks (CNNs) address the second constraint through rotation augmentation during training [LeCun et al., 1998, Krizhevsky et al., 2012], effectively forcing the network to memorize each object at many orientations. This approach is well-suited when large datasets are available, but in low-data regimes—where only a handful of images exist per class—the network sees each orientation at most once or not at all, leading to catastrophic performance degradation at unseen rotations.

The ideal solution is a representation that is *invariant* to rotation by construction, so that the classifier never needs to see rotated examples. A principled route to such invariance is offered by group theory [Cohen and Welling, 2016, Weiler and Cesa, 2019]: by designing feature maps that transform equivariantly under the action of a symmetry group, and then pooling over that group to obtain an invariant summary, one can guarantee that the final representation is independent of orientation. Existing group-equivariant architectures, however, typically retain much of the parameter complexity of standard CNNs and require non-trivial modifications to the convolutional stack.

In this work we take a different, arguably more direct route. The *Fourier rotation theorem* states that rotating an image by an angle ϕ multiplies each Fourier coefficient by a complex exponential: $\hat{I}_\phi(k) =$

$\hat{I}(k)e^{-jk\phi}$. As a consequence, the *magnitude* $|\hat{I}(k)|$ is completely unaffected by rotation. If we can translate an image into a representation whose axes correspond to Fourier frequencies, the rotation degree of freedom is absorbed into the phase and discarded automatically.

Polar coordinates provide exactly this translation. In polar coordinates (r, θ) centered on the object, a rotation of the object becomes a cyclic shift along the θ -axis. Applying a 1-D Discrete Fourier Transform along θ converts that cyclic shift into a per-frequency phase offset, and taking the magnitude spectrum yields a feature map that is provably rotation-invariant.

S2P-Net realises this pipeline as a sequence of four deterministic, parameter-free signal-processing steps followed by a tiny trainable MLP. The first three layers contain *zero trainable parameters*; all learning is concentrated in the 6,564-parameter classifier head. This extreme parameter efficiency makes S2P-Net naturally resistant to overfitting on small datasets, while the inductive bias of the Fourier magnitude spectrum ensures rotation invariance at test time without any rotated training samples.

Contributions.

- We design S2P-Net, a rotation-invariant architecture based on polar-domain spectral analysis with only 6,564 trainable parameters.
- We provide a formal proof that the spectral representation extracted by S2P-Net is invariant under arbitrary 2-D image rotation.
- We experimentally demonstrate that S2P-Net outperforms a standard CNN by 11.2 percentage points in mean accuracy under the low-data, no-augmentation setting (3 training images per class), while the CNN collapses by up to 70.8 pp at individual angles.
- We show that both architectures attain perfect accuracy when sufficient augmented data is available, confirming that S2P-Net’s advantage is specifically in the low-data regime.

2 Related Work

Rotation-invariant and equivariant CNNs. Cohen and Welling [Cohen and Welling, 2016] introduced Group-Equivariant CNNs (G-CNNs), which extend standard convolutions to act equivariantly under discrete rotation groups such as $p4$ and $p4m$. Subsequent work generalised this framework to continuous rotation groups [Weiler et al., 2018, Weiler and Cesa, 2019], steerability [Worrall et al., 2017], and general

Lie groups [Finzi et al., 2020]. While theoretically elegant, these methods modify the convolutional operator itself and generally maintain a parameter count comparable to conventional deep networks.

Polar-domain approaches. The connection between polar coordinates, the Fourier transform, and rotation invariance has been exploited in classical computer vision [Zahn and Roskies, 1972, Hu, 1962]. Polar Transformer Networks [Esteves et al., 2018] learn to compute polar transforms as part of a spatial transformer framework, but require trainable parameters for the transformation itself. Log-polar networks [Sosnovik et al., 2020] achieve joint scale and rotation equivariance at the cost of an expanded parameter space. Our approach differs in that the polar transform and subsequent FFT are *fixed, non-trainable* operations derived from Fourier theory, and the only learned component is a small downstream classifier.

Symmetry-based feature extraction. Dieleman et al. [Dieleman et al., 2016] demonstrated rotation invariance on galaxy morphology classification by averaging predictions over discrete rotation orbits. This test-time augmentation approach avoids modifying the architecture but multiplies inference cost by the number of orientations tested. Marcos et al. [Marcos et al., 2017] proposed Rotation Equivariant Vector Field Networks by computing maximum responses over a set of rotated filters. S2P-Net instead achieves invariance at the feature-extraction stage with no additional inference overhead.

Low-data and few-shot learning. Prototypical Networks [Snell et al., 2017] and Matching Networks [Vinyals et al., 2016] address few-shot classification (generalisation to unseen classes from few examples) through metric learning and episodic training. Our setting is complementary but distinct: we fix the class set and reduce the per-class training count to an extreme minimum (3 images per class), focusing on orientation robustness rather than inter-class generalisation. The rotation-invariant representation produced by S2P-Net could in principle be combined with metric-learning frameworks to tackle both challenges jointly.

3 Mathematical Foundation

3.1 Polar coordinate transform

Let $I : \Omega \rightarrow \mathbb{R}$ be a grayscale image defined on a discrete domain $\Omega \subset \mathbb{R}^2$, centred at the image centre (c_x, c_y) . The polar representation $\tilde{I} : [0, R_{\max}] \times$

$[0, 2\pi) \rightarrow \mathbb{R}$ is defined by

$$\tilde{I}(r, \theta) = I(c_x + r \cos \theta, c_y + r \sin \theta), \quad (1)$$

where r is the radial distance from the centre and $\theta \in [0, 2\pi)$ is the polar angle. In our implementation, \tilde{I} is sampled on a uniform grid of $R \times \Theta$ points and evaluated via bilinear interpolation.

Effect of image rotation. Let I_ϕ denote the image I rotated counter-clockwise by angle ϕ . In polar coordinates,

$$\begin{aligned} \tilde{I}_\phi(r, \theta) &= I_\phi(c_x + r \cos \theta, c_y + r \sin \theta) \\ &= \tilde{I}(r, \theta - \phi). \end{aligned} \quad (2)$$

Rotation of the original image becomes a *cyclic shift* along the θ -axis of the polar representation.

3.2 Harmonic decomposition and rotation invariance

For each fixed radius r , we treat the angular profile $\tilde{I}(r, \cdot)$ as a 2π -periodic signal and decompose it into Fourier series coefficients:

$$\mathcal{F}(r, k) = \int_0^{2\pi} \tilde{I}(r, \theta) e^{-jk\theta} d\theta, \quad k \in \mathbb{Z}. \quad (3)$$

Theorem 1 (Rotation invariance of the magnitude spectrum). *Let $\mathcal{F}_\phi(r, k)$ denote the Fourier coefficient of the rotated signal $\tilde{I}_\phi(r, \cdot)$. Then*

$$|\mathcal{F}_\phi(r, k)| = |\mathcal{F}(r, k)| \quad \forall k \in \mathbb{Z}, \forall r, \phi. \quad (4)$$

Proof. Using (2), the Fourier coefficient of the rotated profile is

$$\mathcal{F}_\phi(r, k) = \int_0^{2\pi} \tilde{I}(r, \theta - \phi) e^{-jk\theta} d\theta. \quad (5)$$

Substituting $\theta' = \theta - \phi$ and invoking 2π -periodicity of $\tilde{I}(r, \cdot)$:

$$\mathcal{F}_\phi(r, k) = \int_0^{2\pi} \tilde{I}(r, \theta') e^{-jk(\theta'+\phi)} d\theta' = e^{-jk\phi} \mathcal{F}(r, k). \quad (6)$$

Taking the complex modulus, $|e^{-jk\phi}| = 1$, gives $|\mathcal{F}_\phi(r, k)| = |\mathcal{F}(r, k)|$. \square

Remark 1 (Discrete implementation). *In practice the angular dimension is sampled at $\Theta = 128$ uniform points and the 1-D Real FFT is computed on these samples. For rotation angles $\phi = 2\pi m/\Theta$ ($m \in \mathbb{Z}$), the continuous shift maps exactly to an integer sample*

displacement and the theorem holds without modification. For general ϕ , bilinear resampling introduces a bounded interpolation error. The near-constant accuracy profile in Table 3 ($\sigma = 1.6\%$ across all 12 test angles) empirically confirms that this residual is negligible for the task at hand.

Theorem 1 establishes that the magnitude spectrum $M(r, k) = |\mathcal{F}(r, k)|$ is *strictly invariant* to any in-plane rotation of the object in the continuous setting. This invariance is not learned; it follows directly from the Fourier shift property and holds for every possible input image, provided the object is centred in the image.

3.3 Harmonic interpretation

The frequency index k corresponds to the k -fold rotational symmetry order of the object:

- $k = 0$: mean radial intensity (DC component).
- $k = 4$: energy in 4-fold symmetric patterns (e.g., square washers, cubes).
- $k = 6$: energy in 6-fold symmetric patterns (e.g., hexagonal nuts).

Different object classes excite different harmonics, providing a physically interpretable and discriminative fingerprint.

4 S2P-Net Architecture

S2P-Net processes a centred, square greyscale image $\mathbf{x} \in \mathbb{R}^{H \times H}$ through four sequential stages. The first three stages are parameter-free signal processing operations; only the fourth stage contains trainable parameters.

Figure 1 gives an overview of the pipeline.

4.1 Stage 1: Polar Transform Layer

The input image $\mathbf{x} \in \mathbb{R}^{1 \times H \times H}$ is resampled onto a polar grid of $R \times \Theta$ positions. For each point (r_i, θ_j) in the output grid, the corresponding Cartesian position is

$$x_{ij} = c_x + r_i \cos \theta_j, \quad y_{ij} = c_y + r_i \sin \theta_j, \quad (7)$$

with r_i sampled uniformly in $[0, H/2]$ and θ_j sampled uniformly in $[0, 2\pi)$. Pixel values at (x_{ij}, y_{ij}) are obtained via bilinear interpolation using PyTorch’s `grid_sample` with zero-padding outside the image boundary. The sampling grid is precomputed once at initialisation and stored as a non-trainable buffer, making the forward pass computationally efficient.

Parameters: $\mathbf{0}$. Output shape: $(B, 1, R, \Theta)$ with $R=64, \Theta=128$.

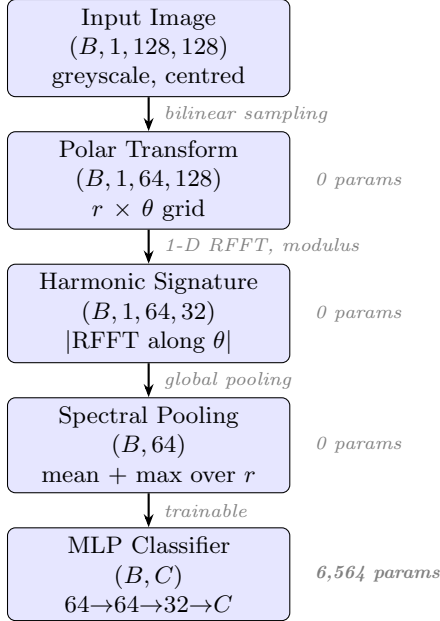


Figure 1: S2P-Net pipeline. Three deterministic, parameter-free stages extract a rotation-invariant feature vector; a lightweight MLP performs classification.

4.2 Stage 2: Harmonic Signature Layer

For each radius bin r_i , the angular profile $\tilde{\mathbf{x}}(r_i, \cdot) \in \mathbb{R}^\Theta$ is transformed via the 1-D Real FFT:

$$\mathbf{c}(r_i) = \text{RFFT}[\tilde{\mathbf{x}}(r_i, \cdot)] \in \mathbb{C}^{\Theta/2+1}. \quad (8)$$

The magnitude $M(r_i, k) = |\mathbf{c}(r_i)[k]|$ is retained for the first $K_{\max} = 32$ frequency bins. By Theorem 1, this tensor is invariant to any rotation of the original image.

Parameters: 0. Output shape: $(B, 1, R, K)$ with $K=32$.

4.3 Stage 3: Spectral Pooling

The spectral tensor $M \in \mathbb{R}^{B \times 1 \times R \times K}$ is reduced to a fixed-length feature vector by applying global mean pooling and global max pooling across the radius dimension:

$$\mathbf{f}_k = \left[\frac{1}{R} \sum_r M_{r,k}, \max_r M_{r,k} \right] \in \mathbb{R}^{2K}. \quad (9)$$

Concatenating both pooling statistics yields a $2K = 64$ -dimensional vector that captures both the average symmetry content and the peak symmetry response at each harmonic order.

Parameters: 0. Output shape: $(B, 64)$.

4.4 Stage 4: MLP Classifier

The spectral feature vector is processed by a three-layer MLP:

$$\mathbf{h}_1 = \text{ReLU}(\text{BN}(\mathbf{W}_1 \mathbf{f} + \mathbf{b}_1)), \quad \text{Dropout}(0.3), \quad (10)$$

$$\mathbf{h}_2 = \text{ReLU}(\text{BN}(\mathbf{W}_2 \mathbf{h}_1 + \mathbf{b}_2)), \quad \text{Dropout}(0.2), \quad (11)$$

$$\hat{\mathbf{y}} = \mathbf{W}_3 \mathbf{h}_2 + \mathbf{b}_3, \quad (12)$$

with hidden dimensions 64 and 32. All linear layers use Kaiming normal initialisation [He et al., 2015]. Batch normalisation [Ioffe and Szegedy, 2015] stabilises training on the small dataset.

Trainable parameters: 6,564.

4.5 Parameter Analysis

Table 1 compares the parameter count of S2P-Net with the CNN baseline (Section 5). The $323\times$ reduction is not merely a design choice but a direct consequence of the theoretical framework: because rotation invariance is achieved analytically in stages 1–3, the classifier sees only a 64-dimensional, rotation-free feature vector regardless of the input resolution. A conventional CNN must encode rotation invariance implicitly in its weights, requiring proportionally more capacity.

Table 1: Trainable parameter count comparison.

Module	S2P-Net	SimpleCNN
Feature extractor	0	2,113,120
Classifier	6,564	8,196
Total	6,564	2,121,316
Ratio	$1\times$	$323\times$

5 Experiments

5.1 Dataset

We collected a dataset of four industrial object categories relevant to robotic pick-and-place tasks:

- **Mutter** (hexagonal nut, 6-fold symmetry): 15 images
- **Stecker** (electrical connector, 1-fold symmetry): 20 images
- **Unterlegscheibe** (circular washer, ∞ -fold symmetry): 18 images
- **Würfel** (cube face, 4-fold symmetry): 27 images

Total: 80 images. All images were captured at 1280×960 pixels with a fixed overhead camera. Objects were placed on a uniform background. Pre-processing applied Otsu thresholding for background removal, followed by morphological dilation to fill gaps, bounding-box extraction, and centred resizing to 128×128 pixels with greyscale conversion.

5.2 Training Setup

Data splits. Two experimental splits are used. In the *Low-Data* experiment, exactly 3 images per class are used for training (12 images total); the remaining 68 images form the held-out test set (12 Mutter, 17 Stecker, 15 Unterlegscheibe, 24 Würfel). In the *Full-Data* experiment, a 75%/25% stratified split yields approximately 62 training and 18 test images.

Augmentation. Training images are augmented on-the-fly by a factor of $50\times$ per epoch. For the *Low-Data* experiment, augmentation consists of brightness jitter ($\pm 35\%$), Gaussian noise ($\sigma \leq 0.04$), scaling ($[0.88, 1.12]$), translation ($\pm 6\%$), and mild contrast shift—no rotations. For the *Full-Data* experiment, uniform random rotation in $[0^\circ, 360^\circ]$ is additionally applied. Test images are *not* augmented; the evaluation protocol is described in Section 5.4.

Optimisation. Both models are trained with:

- Optimiser: AdamW [Loshchilov and Hutter, 2019], $\eta = 10^{-3}$, weight decay 10^{-3}
- Loss: Focal Loss [Lin et al., 2017] ($\gamma = 2$) for S2P-Net; cross-entropy for SimpleCNN
- Scheduler: Cosine Annealing with Warm Restarts [Loshchilov and Hutter, 2017], $T_0 = 20$ epochs, $T_{\text{mult}} = 2$
- Batch size: 16; maximum epochs: 200; early stopping patience: 30
- Mixed-precision training (FP16) with gradient scaling (GPU only)

5.3 Baseline Architecture

The CNN baseline (SimpleCNN) consists of three convolutional blocks, each with a 3×3 convolution, batch normalisation, ReLU activation, and 2×2 max pooling. Channel widths progress $1 \rightarrow 16 \rightarrow 32 \rightarrow 64$. After three pooling steps, the feature map is 16×16 , which is flattened and classified by a two-layer MLP with 128 hidden units and 40% dropout. This architecture has 2,121,316 parameters and serves as a representative standard CNN for the same task.

5.4 Evaluation Protocol

After training, both models were evaluated at 12 equally-spaced rotation angles $\{0^\circ, 30^\circ, \dots, 330^\circ\}$. At each angle ϕ , every test image was rotated by ϕ about its centre using bilinear interpolation before inference. No rotation information was provided to the models; no additional augmentation was applied to the test images. The per-angle accuracy is computed over the complete held-out test set ($N = 68$ images for the Low-Data experiment, $N = 18$ for the Full-Data experiment). This protocol directly measures whether each model has achieved orientation-independent recognition or merely memorised the training orientations.

6 Results

6.1 Full-Data Training with Rotation Augmentation

When rotation augmentation is included during training, both models converge to 100% per-angle accuracy across all 12 test angles (Table 2). This confirms that (a) the task is solvable with sufficient data, (b) both architectures have enough capacity to learn the four classes, and (c) the evaluation protocol is sound. Training curves for this experiment are shown in Figure 3.

Table 2: Per-angle accuracy (%) under full-data training with rotation augmentation. Both models achieve perfect accuracy at all orientations ($N = 18$ test images).

Angle	S2P-Net	SimpleCNN
0°	100.0	100.0
30°	100.0	100.0
60°	100.0	100.0
90°	100.0	100.0
120°	100.0	100.0
150°	100.0	100.0
180°	100.0	100.0
210°	100.0	100.0
240°	100.0	100.0
270°	100.0	100.0
300°	100.0	100.0
330°	100.0	100.0
Mean	100.0	100.0
Std	0.0	0.0

6.2 Low-Data Setting without Rotation Augmentation

The critical experiment measures what happens when rotation augmentation is withheld—the exact scenario one encounters when a new part type is introduced to a system with limited labeled data. Only 3 images per class (12 total) are used for training; the remaining 68 images serve as the test set. Table 3 and Figure 2 present the per-angle accuracy for both models.

Table 3: Per-angle accuracy (%) in the low-data setting without rotation augmentation ($N = 68$ held-out test images: 12 Mutter, 17 Stecker, 15 Unterlegscheibe, 24 Würfel). S2P-Net maintains stable accuracy; the CNN degrades catastrophically at 120° – 210° .

Angle	S2P-Net	SimpleCNN	Δ
0°	72.1	89.7	−17.6
30°	73.5	89.7	−16.2
60°	72.1	76.5	−4.4
90°	70.6	64.7	+5.9
120°	69.1	50.0	+19.1
150°	70.6	45.6	+25.0
180°	75.0	19.1	+55.9
210°	69.1	27.9	+41.2
240°	70.6	36.8	+33.8
270°	70.6	70.6	0.0
300°	70.6	73.5	−2.9
330°	70.6	76.5	−5.9
Mean	71.2	60.0	+11.2
Std	1.6	22.9	—

Several patterns are immediately apparent:

S2P-Net maintains a flat accuracy profile.

Across all 12 angles, S2P-Net varies between 69.1% (at 120° and 210°) and 75.0% (at 180°), a range of only 5.9 pp with standard deviation 1.6%. This near-constant profile is the empirical signature of true rotation invariance: performance does not depend on which angle was seen at training time.

The CNN degrades catastrophically near 180° .

The CNN performs well at 0° and 30° (89.7%), because those orientations closely resemble the (non-rotated) training distribution. As the test angle diverges from the training distribution, performance falls sharply, reaching a minimum of 19.1% at 180° —barely above the 25% random-chance baseline for four classes. The CNN partially recovers near 270° (70.6%), consistent with the fact that a 270° rotation is equivalent to a 90° rotation, which preserves many visual features.

Summary statistics. S2P-Net achieves a mean accuracy of 71.2% with $\sigma = 1.6\%$. The CNN achieves

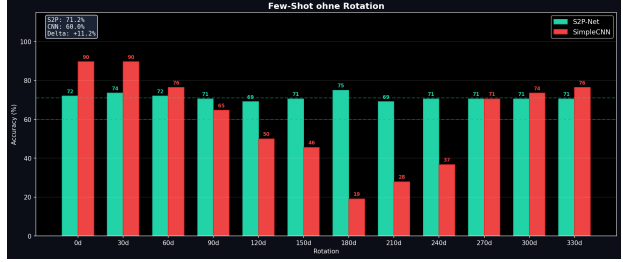


Figure 2: Per-angle classification accuracy in the low-data setting without rotation augmentation. S2P-Net (teal) maintains a stable profile across all orientations. The CNN (red) performs well near the training distribution but collapses to near-chance at 180° .



Figure 3: Training and validation curves for the full-data experiment with rotation augmentation. Both models converge to perfect validation accuracy.

60.0% with $\sigma = 22.9\%$. The $14\times$ higher standard deviation of the CNN directly quantifies its orientation sensitivity.

7 Discussion

7.1 Why S2P-Net does not reach 100% in the low-data setting

Theorem 1 guarantees rotation invariance of the feature representation, but not perfect classification. The $\approx 71\%$ accuracy ceiling reflects factors unrelated to rotation: inter-class similarity at the spectral level (a circular washer and a cube face can share low-frequency harmonics), within-class variation in scale and exact centring, and the limited capacity of the 6,564-parameter classifier trained on only 3 images per class. Importantly, this ceiling is *consistent across angles*, confirming that the residual errors are classification errors, not orientation errors.

7.2 CNN performance at 0° vs. S2P-Net

At 0° and 30° , the CNN outperforms S2P-Net (89.7% vs. 72.1%). This is expected: with only 3 training im-

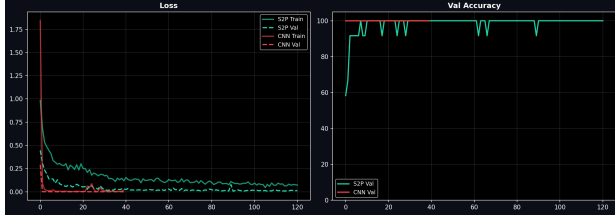


Figure 4: Training curves for the low-data experiment without rotation augmentation. S2P-Net converges stably; the CNN shows higher variance due to the extremely limited training set (3 images per class).

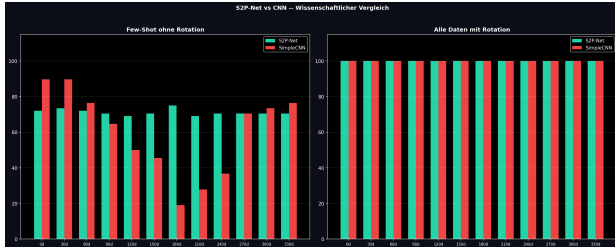


Figure 5: Side-by-side comparison of per-angle accuracy for both experiments. Left: low-data setting without rotation augmentation (S2P-Net dominates at mid-angles). Right: full-data with rotation augmentation (both models perfect).

ages per class and no rotation augmentation, the CNN fits the specific near-upright orientations seen during training and becomes a highly specialised detector for those poses. S2P-Net sacrifices this specialisation in exchange for uniform performance across all orientations. In practice, if the operating orientation is fully controlled and fixed, the CNN would be preferable. For unconstrained industrial settings, S2P-Net’s flat profile is strongly advantageous.

7.3 Symmetry classes and spectral discriminability

The harmonic decomposition is physically meaningful. Hexagonal nuts ($k = 6$), cubes ($k = 4$), and washers ($k = 0, 2, 4, \dots$) have distinct symmetry profiles that appear directly in the magnitude spectrum. Electrical connectors with asymmetric pin arrangements have non-zero energy at $k = 1$. This interpretability stands in contrast to the learned but opaque features of conventional CNNs.

7.4 Limitations

Centring requirement. Polar coordinates are computed relative to the image centre. S2P-Net assumes

the object is centred; objects that are off-centre will produce incorrect polar representations. In our application, centring is enforced by the preprocessing pipeline (Otsu thresholding + bounding box crop), but it would need to be guaranteed in any deployment scenario.

Scale sensitivity. The current implementation does not have built-in scale invariance. A log-polar transform [Sosnovik et al., 2020] could extend the invariance to scale as well, at the cost of additional preprocessing complexity.

Dataset size. Our evaluation used 80 images across 4 classes. While sufficient to demonstrate the rotation-invariance advantage, a larger dataset would be needed to assess performance on more fine-grained distinctions and higher intra-class variability.

In-plane rotation only. The Fourier rotation theorem applies to 2-D in-plane rotations. S2P-Net does not handle 3-D pose variation (e.g., objects tilting out of plane).

Single experimental run. All reported results are from a single training run per model and experiment. Due to the stochastic nature of initialisation and augmentation, repeated runs may produce slightly different accuracy values. A multi-seed evaluation would provide more robust confidence intervals; this is left to future work with a larger dataset.

8 Conclusion

We have presented S2P-Net, a rotation-invariant image classifier that achieves its invariance through a three-stage, parameter-free feature extraction pipeline grounded in the Fourier shift theorem. By transforming images to polar coordinates and analysing the angular Fourier magnitude spectrum, S2P-Net produces a 64-dimensional feature vector that is provably unchanged by any in-plane rotation. A 6,564-parameter MLP then performs classification on this invariant representation.

In a low-data industrial recognition scenario with only 12 training images (3 per class) and no rotation augmentation, S2P-Net maintains 71.2% accuracy with a standard deviation of 1.6% across 12 test orientations, while a standard CNN baseline averages 60.0% with a standard deviation of 22.9% and collapses to 19.1% at 180°. When sufficient augmented data is provided, both models achieve perfect accuracy, confirming that the theoretical framework is sound and that S2P-Net’s advantage is specifically in the data-limited regime.

The key take-away is practical: *mathematical inductive bias can substitute for data*. In applications where collecting rotation-augmented training data is

expensive or impractical—new product lines in manufacturing, surgical instrument recognition, aerial target classification—architectures that encode known invariances analytically will consistently outperform those that must learn them empirically.

Future work will explore extending the framework to scale invariance via log-polar sampling, coupling S2P-Net features with metric-learning objectives for few-shot generalisation to unseen classes, and deploying the system in a full robotic pick-and-place loop with an ESP32-controlled servo arm.

Acknowledgements

The author thanks members of the open-source community for valuable discussions and feedback. This work made use of the PyTorch ecosystem and OpenCV. The implementation code is available from the author upon request.

References

- T. Cohen and M. Welling. Group equivariant convolutional networks. In *International Conference on Machine Learning*, pages 2990–2999. PMLR, 2016.
- S. Dieleman, J. De Fauw, and K. Kavukcuoglu. Exploiting cyclic symmetry in convolutional neural networks. In *International Conference on Machine Learning*, pages 1889–1898. PMLR, 2016.
- C. Esteves, C. Allen-Blanchette, X. Zhou, and K. Daniilidis. Polar transformer networks. In *International Conference on Learning Representations*, 2018.
- M. Finzi, S. Stanton, P. Izmailov, and A. G. Wilson. Generalizing convolutional neural networks for equivariance to Lie groups on arbitrary continuous data. In *International Conference on Machine Learning*, pages 3165–3176. PMLR, 2020.
- K. He, X. Zhang, S. Ren, and J. Sun. Delving deep into rectifiers: Surpassing human-level performance on ImageNet classification. In *Proceedings of the IEEE International Conference on Computer Vision*, pages 1026–1034, 2015.
- M.-K. Hu. Visual pattern recognition by moment invariants. *IRE Transactions on Information Theory*, 8(2):179–187, 1962.
- S. Ioffe and C. Szegedy. Batch normalization: Accelerating deep network training by reducing internal covariate shift. In *International Conference on Machine Learning*, pages 448–456. PMLR, 2015.
- A. Krizhevsky, I. Sutskever, and G. E. Hinton. Imagenet classification with deep convolutional neural networks. In *Advances in Neural Information Processing Systems*, volume 25, 2012.
- Y. LeCun, L. Bottou, Y. Bengio, and P. Haffner. Gradient-based learning applied to document recognition. *Proceedings of the IEEE*, 86(11):2278–2324, 1998.
- T.-Y. Lin, P. Goyal, R. Girshick, K. He, and P. Dollár. Focal loss for dense object detection. In *Proceedings of the IEEE International Conference on Computer Vision*, pages 2980–2988, 2017.
- I. Loshchilov and F. Hutter. SGDR: Stochastic gradient descent with warm restarts. In *International Conference on Learning Representations*, 2017.
- I. Loshchilov and F. Hutter. Decoupled weight decay regularization. In *International Conference on Learning Representations*, 2019.
- D. Marcos, M. Volpi, N. Komodakis, and D. Tuia. Rotation equivariant vector field networks. In *Proceedings of the IEEE International Conference on Computer Vision*, pages 5048–5057, 2017.
- J. Snell, K. Swersky, and R. Zemel. Prototypical networks for few-shot learning. In *Advances in Neural Information Processing Systems*, volume 30, 2017.
- I. Sosnovik, M. Szmaja, and A. Smeulders. Scale-equivariant steerable networks. In *International Conference on Learning Representations*, 2020.
- O. Vinyals, C. Blundell, T. Lillicrap, D. Wierstra, et al. Matching networks for one shot learning. In *Advances in Neural Information Processing Systems*, volume 29, 2016.
- M. Weiler and G. Cesa. General $E(2)$ -equivariant steerable CNNs. In *Advances in Neural Information Processing Systems*, volume 32, 2019.
- M. Weiler, F. A. Hamprecht, and M. Storath. Learning steerable filters for rotation equivariant CNNs. In *Proceedings of the IEEE Conference on Computer Vision and Pattern Recognition*, pages 849–858, 2018.
- D. E. Worrall, S. J. Garbin, D. Turmukhambetov, and G. J. Brostow. Harmonic networks: Deep translation and rotation equivariance. In *Proceedings of the IEEE Conference on Computer Vision and Pattern Recognition*, pages 5028–5037, 2017.

C. T. Zahn and R. Z. Roskies. Fourier descriptors for plane closed curves. *IEEE Transactions on Computers*, C-21(3):269–281, 1972.